Applied Catalysis B: Environmental 88 (2009) 232–239

Contents lists available at ScienceDirect

Applied Catalysis B: Environmental

journal homepage: www.elsevier.com/locate/apcatb

Photocatalytic oxidation of ethylene by ammonium exchanged ETS-10 and AM-6

Michael J. Nash [a], Raul F. Lobo [a,*], Douglas J. Doren [b]

[a] Department of Chemical Engineering, Center for Catalytic Science and Technology, University of Delaware, 150 Academy St., Newark, DE 19716, USA
[b] Department of Chemistry and Biochemistry, University of Delaware, Newark, DE 19716, USA

ARTICLE INFO

Article history:
Received 12 June 2008
Received in revised form 28 August 2008
Accepted 3 October 2008
Available online 14 October 2008

Keywords:
ETS-10
Transition metal doping
AM-6
Photocatalysis
Band gap energy
Environmental catalysis

ABSTRACT

ETS-10 and AM-6 in the as-prepared and ammonium form have been characterized using Raman, X-ray powder diffraction, N_2 adsorption, energy dispersive X-ray (EDX) analysis, UV/vis spectroscopy, and diffuse reflectance infrared Fourier transform spectroscopy (DRIFTS). Upon NH_4^+ ion exchange, AM-6 shows the loss of the characteristic V–O–V stretch in the Raman spectrum similar to the effects observed for NH_4^+ ion exchanged ETS-10. The UV/vis spectrum of NH_4^+ ion exchanged AM-6 also shows similar changes to NH_4^+ ion exchanged ETS-10, though the band gap in AM-6 is not red shifted as it is in ETS-10. Heating the NH_4^+ exchanged AM-6 to form H-AM-6 changes the coordination environment of the vanadium from an octahedral coordination to a tetrahedral coordination, but does not cause the partial collapse of the AM-6 structure. The oxidation of ethylene under oxygen on as-synthesized AM-6 only produces partial oxidation products while the NH_4^+ ion exchanged AM-6 was able to completely oxidize ethylene to CO_2.

1. Introduction

Increasing concerns about new organic contaminants, such as pharmaceuticals and endocrine-disrupting compounds [1] that may not be decomposed with conventional water treatment methods such as biological treatment, will require new and effective methods for purification. To this end, semiconductor photocatalysts offer promising possibilities. Interest in semiconductors as photocatalysts for the decomposition of volatile organic compounds (VOCs) in wastewater and other media is long standing and commercial applications based on semiconductor photocatalysts are beginning to emerge [2,3]. The majority of these applications are based on solar collectors which focus sun's light into clear plug-flow reactors that contain the wastewater and the photocatalyst. The photocatalyst used in most of these solar collectors is TiO_2 since it is inexpensive, nontoxic, and has a relatively high reactivity for the decomposition of VOCs [4,5].

TiO_2 has disadvantages that must be overcome if these applications are to gain widespread industrial use. First, TiO_2 is a wide-gap semiconductor with a band gap energy of 3.2 eV for the anatase phase, which means that electron–hole pairs are only created when it is exposed ultraviolet (UV) light [5]. Since a small percentage of the solar spectrum consists of high energy UV light, the majority of the electromagnetic radiation collected by the solar collectors is lost as heat. An ideal photocatalyst would need to absorb visible light in order to make more efficient use of the solar radiation. Second, an electron–hole pair created from a UV photon in TiO_2 does not necessarily catalyze a reaction since carrier recombination throughout the catalyst particle is a possible reaction path. New photocatalysts with lower recombination rates would have higher reactive quantum yield. Several groups are developing new methods, such as metal ion doping to address this problem [5–8]. Alternatively, since electron and hole transfers to absorbed molecules occur at the surface of a TiO_2 particle, rates can be increased decreasing the TiO_2 particles in size to increase the surface area per unit mass.

A microporous titanosilicate called ETS-10 [9] has the potential to overcome the disadvantages associated with TiO_2. ETS-10 is composed of octahedrally coordinated $TiO_{6/2}$ units that form linear chains by sharing apical oxygen atoms, and are surrounded by corner sharing $SiO_{4/2}$ tetrahedra. The silicate forms a three-dimensional 12-ring pore structure, with an ideal unit cell composition of $(Na, K)_2TiSi_5O_{13}$ [10]. This structure of ETS-10 is complex and has inherent disorder as a result of intergrowth of two polymorphs. Fig. 1 illustrates the structure of one polymorph, polymorph A, along with an enlarged section of the region around one chain and its counter ions.

* Corresponding author. Tel.: +1 302 831 1261; fax: +1 302 831 2085.
E-mail address: lobo@udel.edu (R.F. Lobo).

0926-3373/$ – see front matter © 2008 Elsevier B.V. All rights reserved.
doi:10.1016/j.apcatb.2008.10.001

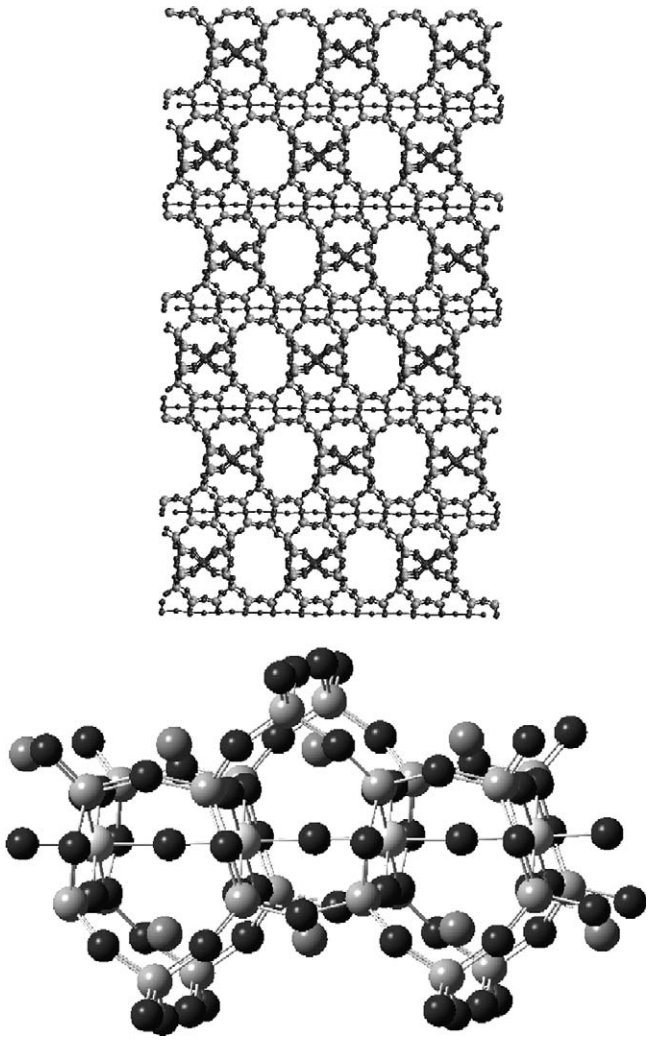

Fig. 1. Polymorph A along the [1 0 0] direction and an enlarged section of the titanium chain of ETS-10 with $SiO_{4/2}$ tetrahedra and Na cations surrounding the $TiO_{6/2}$ units.

Unfortunately, the band gap of ETS-10 is 4.03 eV, which is larger than that of TiO_2 due to the quantum confinement effect on the chain [11]. Several groups have substituted transition metals such as Fe [12], Cr [13], and V [14,15] into the titanium chains in an effort to change the absorbance spectrum of the material. These substitutions reduce the band gap and add new transitions in the visible region ($h\nu > 400$ nm). Uma et al. [16] have shown that the addition of Cr and Co makes ETS-10 active in the visible region after calcination at 500 °C for the decomposition of acetaldehyde. However, Co is believed to be substituting for Si rather than Ti. Substitution by vanadium is unique in that it can completely replace titanium in the chains while still maintaining the same structure. The completely vanadium substituted version of ETS-10 is known as AM-6. In a previous report, we have shown that vanadium-incorporated ETS-10 and AM-6 are active photocatalysts in the visible region for the polymerization of ethylene [17]. Addition of vanadium lowered the band gap energy of ETS-10 and added several new absorbance peaks in the UV/vis spectrum above 400 nm; the peak near 450 nm was photocatalyticly active. These results are consistent with calculations by Shough et al. [18,19] using hybrid DFT/MM methods with cluster models of ETS-10 and AM-6. They showed that the lowering of the band gap with the addition of vanadium results from the addition of delocalized d-orbital states at the bottom of the conduction band.

Addition of metal ions to the ETS-10 structure may also introduce localized states below the conduction band where an electron can be trapped, reducing its chance of recombining with a hole. Hole traps may also be created. These electron–hole traps would thus slow down the rate of electron–hole recombination as long as they are located far from each other. Evidence for this effect has been found by Shough et al. [20] who identified electron/hole trapping sites in vanadium substituted ETS-10 with V^{5+}/V^{4+} species, respectively, both of which are known to be present. The proximity of electron and hole traps to one another will affect recombination rates, and their proximity to the surface will affect the rates of productive photocatalytic reactions.

The specific surface area of ETS-10 and AM-6 is much larger than that of TiO_2. However since the linear chains are surrounded by SiO_2 tetrahedra, the chains are mostly isolated from adsorbed molecules and only a portion of the ETS-10/AM-6 surface area is reactive. The linear chains resemble "quantum wires" where an electron–hole pair can only travel in one dimension and can only react with adsorbed molecules at the termination of the chains or at structural defects where the chains are exposed to adsorbed species. Xamena et al. [21] have explored different post-synthesis techniques such as mild HF treatments as a way of increasing the photoreactivity by inducing defects along the chain. These authors showed that an ad hoc mild treatment of HF to ETS-10 could be used to control the number of defects in the ETS-10 structure and thus its photoactivity for the degradation of large aromatic molecules.

Another method of introducing defects into ETS-10 or AM-6 is through ion exchange. A recent study by Krisnandi et al. [22] showed that NH_4^+ ion exchange on ETS-10 leaves the crystallinity of the structure unchanged but does introduce local defects in the Ti chains. This effect is irreversible: Na^+ ion back-exchange did not repair the defects but instead introduced further defects. Krisnandi et al. also showed that the edges of the crystals of ETS-10 are depleted of silicon and that the Ti coordination begins to resemble that of anatase. These structural changes led to a red shift in the band gap energy of ETS-10. A follow-up study [23] using EPR and FTIR measurements, showed that the defective samples were able to photoreduce Ti and cause the complete oxidation of ethylene to CO_2 in O_2, while the as-synthesized sample were not.

In this report, the effects of NH_4^+ ion exchange on the properties and photoactivity of AM-6 are studied and compared to results with ETS-10. We will show that by using a less concentrated NH_4^+ ion solution for ion exchange, enough defects can be added to the AM-6 structure to change the coordination environment of the vanadium. Also, a more pronounced coordination change is shown upon heating. The AM-6 structure is less stable than that of ETS-10 after the same ion exchange treatment, and the photoreactivity of exchanged AM-6 resembles that of exchanged ETS-10 for the decomposition of ethylene in oxygen.

2. Experimental

2.1. Synthesis, NH_4^+ exchange, and characterization

The synthesis of ETS-10 and AM-6 samples was carried out according to a protocol described previously [17]. After synthesis, 1 g samples of ETS-10 and AM-6 were added to a beaker with 500 ml of 0.1 M NH_4NO_3 and allowed to exchange for approximately 19 h at 70 °C. These samples where then vacuum filtered and dried at room temperature.

Powder X-ray diffraction (XRD), adsorption isotherms, EDX analysis, and UV/vis spectra were all obtained using previously described methods [17]. Band gap energies were determined using the method of Gao and Wachs [24], and a detailed discussion can

be found in our previous study [17]. The percent crystallinity is defined as the ratio of the area under the characteristic peak at 24.4° 2θ in the XRD pattern for a given sample to the area under the same peak for the as-synthesized sample. Raman spectra were collected in ambient air using a diode laser (784.68 nm) with an exposure time of 3 s and an accumulation time of 4 s.

2.2. Photocatalysis

Photocatalytic studies were carried out using a diffuse reflectance infrared Fourier transform spectroscopy (DRIFTS) cell, the details of which can be found elsewhere [17]. All IR spectra were collected from 100 scans at a resolution of 4 cm^{-1} and were obtained at a mirror velocity of 1.90 cm/s.

Ethylene oxidation in O_2 was chosen to compare ETS-10 and AM-6 as photocatalysts for the oxidation of VOCs. In the reactivity tests, the following protocol was used:

(1) Approximately 200 mg of catalyst sample was dehydrated under vacuum for one day at 250 °C in the cell.
(2) After dehydration the sample was cooled to room temperature and a background spectrum was collected.
(3) Ethylene and O_2 were then introduced into the cell in a 1:3 ratio up to a pressure of ~300 Torr and allowed to equilibrate for several minutes.
(4) The UV lamp was turned on and spectra were collected every 2 min for 10 h.
(5) The lamp was turned off and the cell was allowed to equilibrate for 30 min.
(6) The cell was evacuated to remove any gaseous or weakly physisorbed species and a final spectrum was collected.

The source of UV radiation was a 450 W Thermo Oriel Xe arc-lamp and the light was introduced to the sample via a fiber optic cable. The temperature of the samples during irradiation was monitored using a thermocouple and only a small increase in temperature was observed (< 5 °C). The spectrum of the light emitted from the lamp ranges from ~270 nm all the way up into the visible region.

3. Results and discussion

3.1. Characterization

Table 1 shows the (Na + K)/(Ti + V) ratio, unit cell volume, micropore volume, and calculated band gap energies for ETS-10 and AM-6 before and after NH_4^+ ion exchange. The (Na + K)/(Ti + V) ratios taken from EDX show that the initial ratios for the as-synthesized samples are slightly higher than the expected value of 2. After ion exchange, both ETS-10 and AM-6 show a large decrease in the Na and K content as the NH_4^+ ions replace these cations inside the pores; with the larger decrease observed in the ETS-10 sample. The unit cell volume of ETS-10 decreases after ion exchange while the volume of AM-6 remains almost the same. The micropore volumes of both ETS-10 and AM-6 show a slight increase after ion exchange which is expected since the measurements were taken after the samples were thermally treated and the molar volume of the ammonium ion is larger than that of a proton.

The optical spectrum of ETS-10 depends on the degree of order of the $TiO_{6/2}$ chains [25–27]. Previous studies have shown that the absorption edge is made up of two components, a high energy transition at around 250 nm associated with a ligand-to-metal charge transfer (LMCT) from a delocalized orbital on the oxygen atoms to the titanium atom, and a lower energy transition at around 285 nm of the same LMCT only from a localized orbital on the oxygen atoms at defects sites [27]. These localized orbitals on oxygen associated with defect sites have also been assigned to the red shift in the band gap energy observed after ion exchange and acid treatment [22]. These changes have been observed in our ETS-10 samples (Fig. 2A), where NH_4^+ exchange leads to increased absorbance in the 285 nm region along with a red shift in the band gap energy (Table 1). Dehydration of this sample maintains this shift and also increases the baseline in the visible region of the spectrum. The reason for this change in baseline is unknown at this time. The band gap energy of 4.35 eV for as-synthesized ETS-10 is higher than the value previously reported by Borello [11] of 4.03 eV. In this study ETS-10 was synthesized using TiO_2 (anatase) as the titanium source instead of $TiCl_3$ and it has been shown that this leads to better crystallinity of the chains and structure [28,29]. This is also likely to be the reason for the complex shape of the UV/vis spectra for ETS-10 which does not show a sharp edge but instead a broad edge of intensity.

The absorption spectrum of AM-6 is very different from that of ETS-10 and NH_4^+ ion exchange has a different effect. The AM-6 spectrum consists of four absorption features at 300, 450, 594, and >850 nm. (*Note*: that the maximum wavelength detected by the spectrometer is 850 nm.) Shough et al. [18] have assigned the 300 nm and 450 nm features to $O(2p) \rightarrow V(d_{xz}/d_{yz})$ transitions where the bottom of the conduction band is made up of vanadium d orbitals. The feature at 594 nm has been ascribed by others to a d-d transition on the vanadium(IV) atoms in the AM-6 sample [14]. However, Shough et al. [18] suggest that this is a LMCT transition from the O(2p) orbital at the top of the valence band to a $V^V(d_{xy})$ mid-gap state between the conduction band and the valence band. The final feature of the AM-6 spectrum at 850 nm, at the edge of wavelength range of the spectrometer, is assigned to a d-d transition on the vanadium(IV) atoms. Ion exchange has only a small effect on spectral properties of AM-6, causing small increases in the 594 and 850 nm regions but no real shift in the band gap (Fig. 2B and Table 1). There is however, a large change upon dehydration of ion exchanged AM-6 sample, which causes a red shift of the 300 nm peak and a large change in the baseline for the visible region. The large red shift suggests that a change in oxidation state and/or coordination may have occurred with dehydration of the exchanged sample, as is also suggested by the Raman spectra.

Table 1
Ion to metal ratio, unit cell volume, micropore volume, and optical band gap energy of ETS-10 and AM-6 before and after NH_4^+ exchange.

	(Na + K)/(Ti + V)	Unit cell volume (A^3)	Micropore volume (cm^3/g)	Band gap energy (eV)
ETS-10				
Before NH_4^+	2.57 ± 0.17	6121.3	0.145	4.35
After NH_4^+	0.49 ± .005	5955.4	0.160	3.91
AM-6				
Before NH_4^+	2.47 ± 0.13	6000.0	0.134	3.66
After NH_4^+	1.24 ± 0.12	5993.1	0.144	3.70

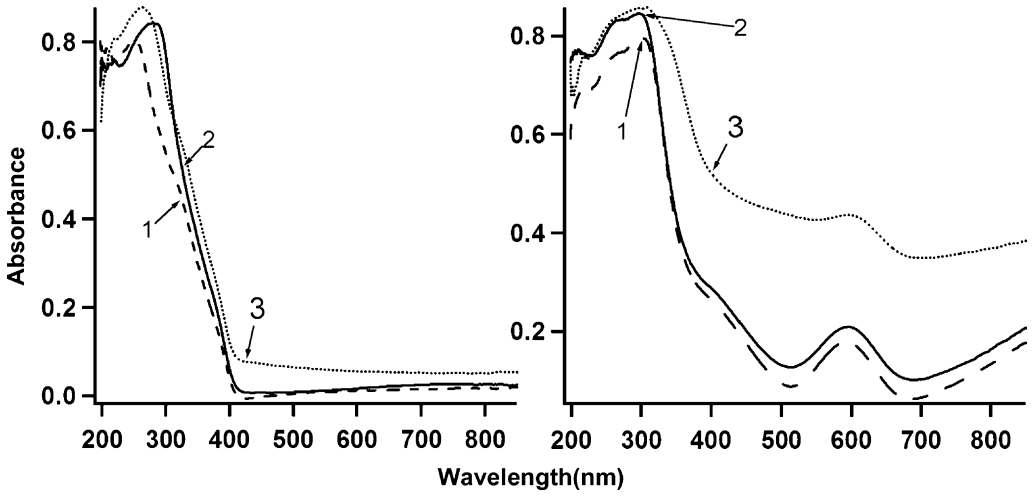

Fig. 2. Change in the UV/vis spectra with NH_4^+ exchange for (A) ETS-10 and (B) AM-6 before NH_4^+ exchange (1), after NH_4^+ exchange (2), and after exchange and dehydration (3).

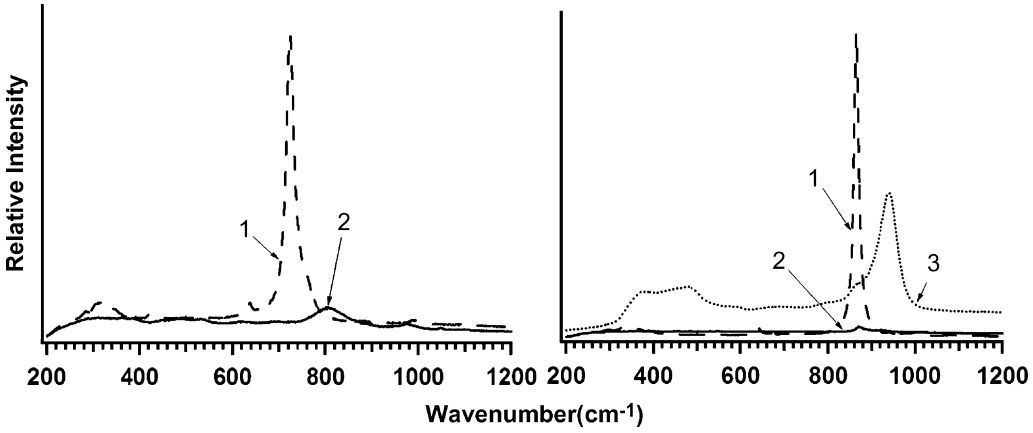

Fig. 3. Change in the Raman spectra with NH_4^+ exchange for (A) ETS-10 and (B) AM-6 before NH_4^+ exchange (1), after NH_4^+ exchange (2), and after exchange and dehydration (3).

NH_4^+ ion exchange dramatically changes the Raman spectra of the ETS-10 and AM-6 samples, as seen in Fig. 3. The Raman spectrum of untreated ETS-10 is dominated by the characteristic Ti-O–Ti stretch along the $TiO_{6/2}$ chain at 727 cm^{-1} which has been used as a measure of order along the chain [26,27]. After ion exchange this band disappears and a very broad weak band around 800 cm^{-1} appears, suggesting that the coordination along the chain has changed with the incorporation of NH_4^+ ions. This broad band has yet to be assigned and could be from the appearance of defective titanium octahedra as has been suggested by Krisnandi et al. [22]. The spectra of exchanged and dehydrated ETS-10 are not shown because only poor and noisy spectra could be obtained for

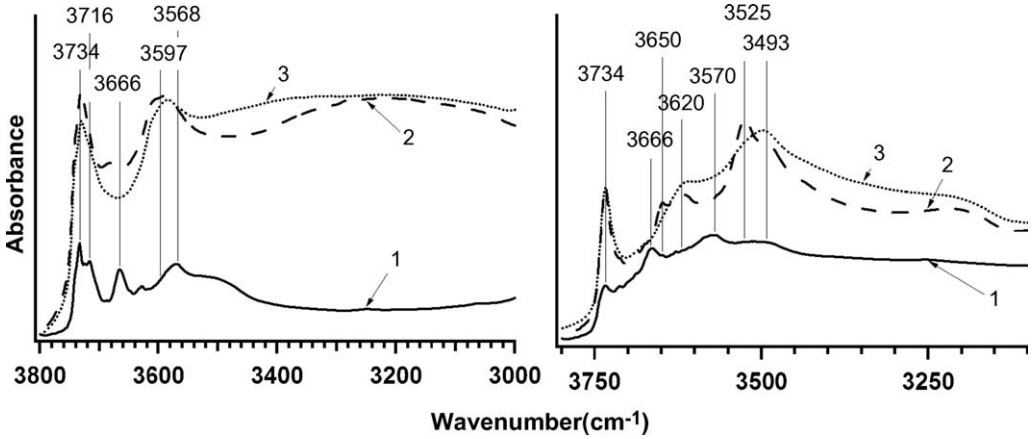

Fig. 4. Creation of new surface sites in the NH_4^+ exchange forms of (A) ETS-10 and (B) AM-6 before NH_4^+ exchange (1), after NH_4^+ exchange (2), and after reaction with C_2H_4 and O_2 (3).

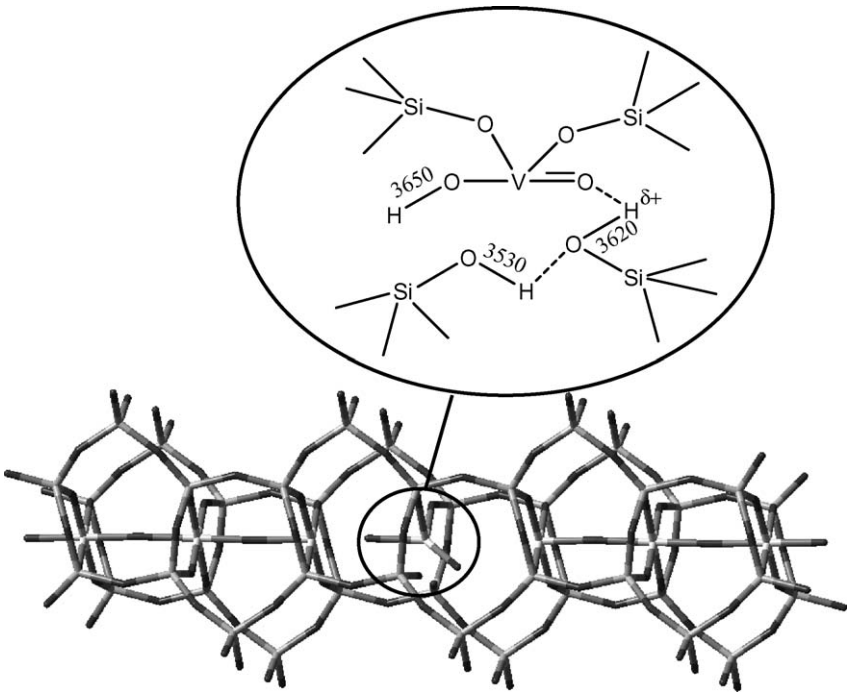

Fig. 5. A possible model for the local coordination environment of vanadium after decomposition of the NH_4^+ ion along with some of the IR stretching frequencies (cm^{-1}) observed.

these samples. The spectrum of untreated AM-6 has an analogous V–O–V stretch peak at 867 cm^{-1} that is narrower than the one for ETS-10 (FWHM of 16.5 cm^{-1} for AM-6 vs. 25.8 cm^{-1} for ETS-10) and suggests a difference in local order along the octahedral chains for AM-6 and ETS-10. The peak does not completely disappear with the NH_4^+ ion treatment. The small peak remaining at 867 cm^{-1} suggests that some of the vanadium in the chain is unaffected after the ammonium exchange. (In mixed vanadium and titanium samples (not shown) the Raman spectra after NH_4^+ exchange still retain a small V–O–V stretch but no Ti–O–Ti stretch.) Although it appears there is a change in coordination with ammonium ion exchange, it does not produce any distinct new Raman features as it does in ETS-10. There is however, a large peak that is formed upon dehydration of the exchanged sample at 939 cm^{-1}. The peak is also present in the as-synthesized sample; however, its intensity is very small. This peak is typical of a V=O bond and has been assigned to this species by Rocha et al. [15].

The change in coordination of the vanadium and titanium atoms in the ETS-10 structure upon ion exchange gives rise to additional OH stretches in the dehydrated IR spectra. In Fig. 4A, the spectrum of dehydrated untreated ETS-10 has four distinct stretches at 3734, 3716, 3666, and 3568 cm^{-1} where the first two are associated with surface SiOH and TiOH stretches, respectively, and the second two with residual water left in the sample. NH_4^+ ions absorb strongly in the 3800–3000 cm^{-1} region, so the exchanged samples have higher absorption throughout the region. In the spectrum of treated ETS-10 after dehydration only two peaks are visible, at 3734 and 3597 cm^{-1}, where the first is associated with SiOH stretches and the second with Si(OH)Ti Brønsted acid sites [30]. Dehydration of the exchanged sample under vacuum above 200 °C causes the NH_4^+ ion to break down, forming ammonia and the acid form of ETS-10/AM-6. The SiOH peak increases and broadens after exchange suggesting that the treatment may have broken Si–O–Si bonds or Si–O–Ti bonds and created new SiOH sites (the TiOH stretches may also be part of this broader peak). These changes to the OH region remain after reaction with ethylene and oxygen.

The spectrum of untreated dehydrated AM-6 has three main peaks at 3734, 3666, and 3570 cm^{-1} which correspond again to SiOH and residual water. NH_4^+ exchange again increases and broadens the SiOH peak. Two new peaks form in the Brønsted acid region at 3650 and 3620 cm^{-1} which have been suggested to be from tetrahedral vanadium with hydroxyl groups (VOH) [31,32]. The 3650 cm^{-1} peak would be from a largely isolated VOH bond while the 3620 cm^{-1} peak would be from a VOH bond experiencing strong interactions from Si. Two peaks appear in the dehydrated ion exchanged AM-6 sample at lower frequency, 3525 and 3493 cm^{-1}, which correspond to hydrogen-bonded internal SiOH groups [33,34]. As in the case for ETS-10, the changes to the OH region remain unaffected by reaction and irradiation.

These new FTIR peaks in the dehydrated, ion-exchanged samples along with the changes in UV/vis spectrum and the

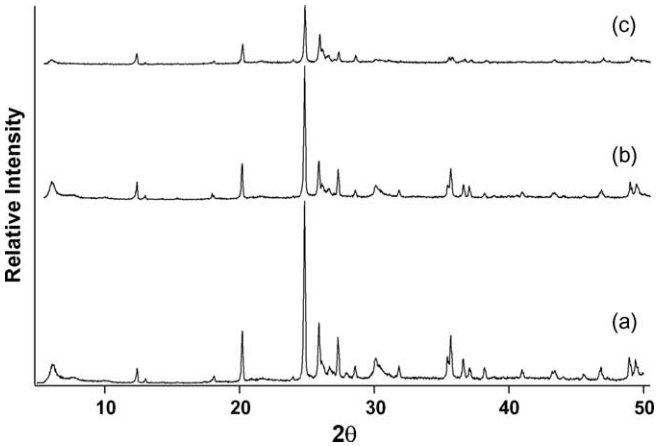

Fig. 6. The X-ray diffraction patterns of AM-6 after (a) synthesis, (b) NH_4^+ ion exchange, and (c) NH_4^+ ion exchange and dehydration.

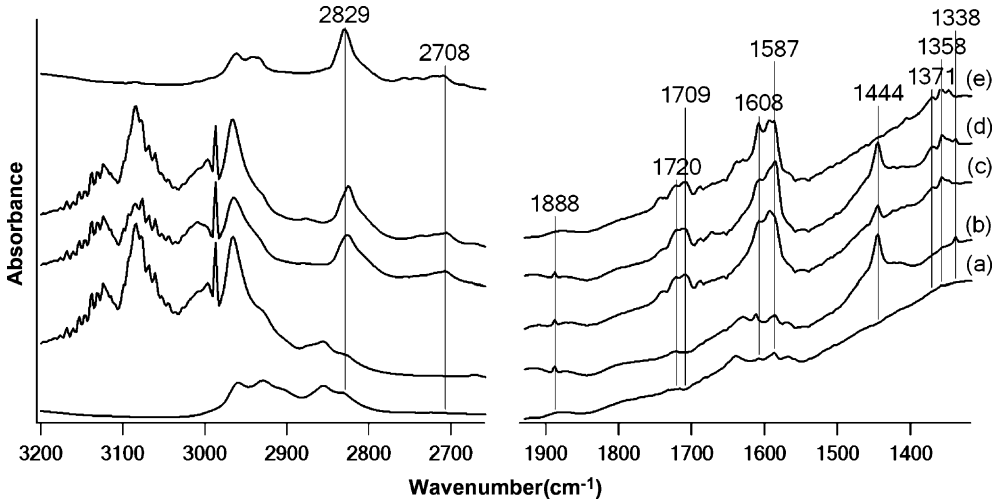

Fig. 7. IR spectra of (CH) and ν(CO) regions for AM-6 (a) under vacuum, (b) with 300 Torr C_2H_4 and O_2 in a 1 to 3 ratio, (c) after 10 h under UV, (d) after 30 min with UV lamp off, and (e) after evacuating reaction chamber.

formation of the V=O bond in the Raman spectrum suggest that upon ammonia desorption, the vanadium in the chains changes its octahedral coordination and begins to adopt a tetrahedral coordination, resembling the coordination of vanadium incorporated in zeolite beta [31]. One possible model for this new configuration can be seen in Fig. 5 where the vanadium is tetrahedrally coordinated and has hydrogen bonding interactions with the SiOH groups.

A large change in vanadium coordination raises doubts about the structural stability of AM-6. Fig. 6 shows the XRD pattern of AM-6 before ion exchange, after ion exchange, and after dehydration and reaction of the ion exchanged samples. It is clear that the crystal structure remains largely intact after ion exchange although there is a substantial reduction in peak intensity. There is however no change in the width of the characteristic peaks for AM-6 in any of the three diffraction patterns and no evidence of amorphous material is present. Further more; the dehydrated sample still has nearly the same micropore volume. These results suggest that the AM-6 structure does not collapse with dehydration and that the change in intensity is due to changes in atomic position that do not include structural collapse. Further structural studies are needed to fully explain these observations.

3.2. Photoreactivity

The IR spectra for the reaction of ethylene with O_2 on as-synthesized ETS-10 are consistent with those previously reported by Krisnandi et al. [35] and are not reported here.

Fig. 7 shows selected IR spectra from the reaction of ethylene with O_2 on untreated AM-6. The peaks above 2900 cm^{-1}, along with the 1444, 1888, and the 1338 cm^{-1} peaks, have been associated with physisorbed ethylene [23,35]. After 10 h under UV light these features slightly decrease and new bands associated with partial oxidation products such as acetaldehyde, acetic acid, and formic acid appear in the ν(C–H), ν(C=O), and ν(CH_3) regions. The peaks in the ν(CH_3) region (1371, 1358 cm^{-1}) and in the ν(C=O) region (1720, 1709 cm^{-1}) may be from a combination of acetic acid and acetaldehyde products [23,35], while the two other

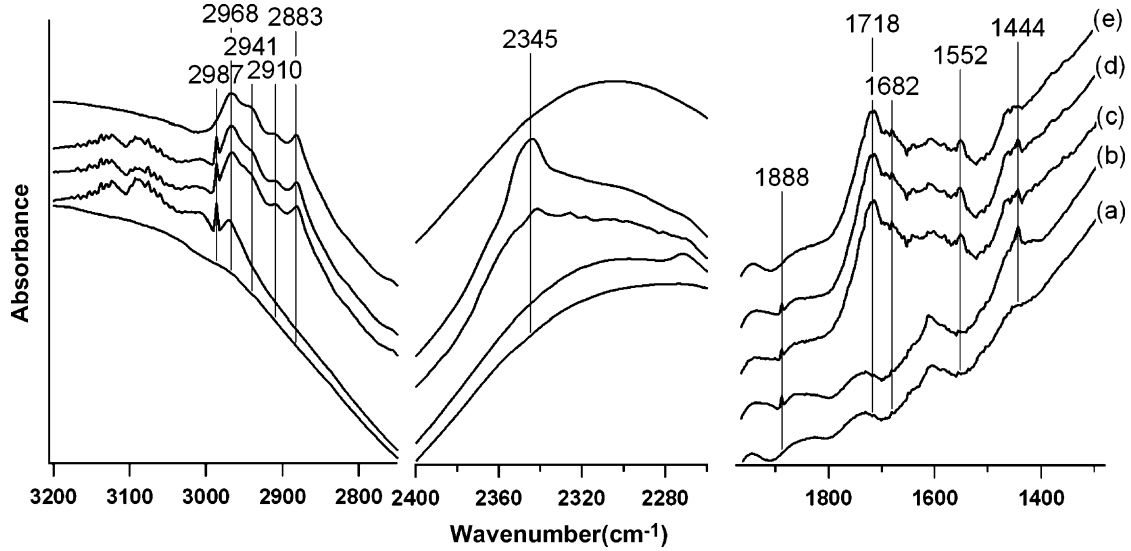

Fig. 8. IR spectra of ν(CH), ν(CO_2), ν(CO) regions for 0.1 M NH_4NO_3 treated ETS-10 (a) under vacuum, (b) with 300 Torr C_2H_4 and O_2 in a 1 to 3 ratio, (c) after 10 h under UV, (d) after 30 min with UV lamp off, and (e) after evacuating reaction chamber.

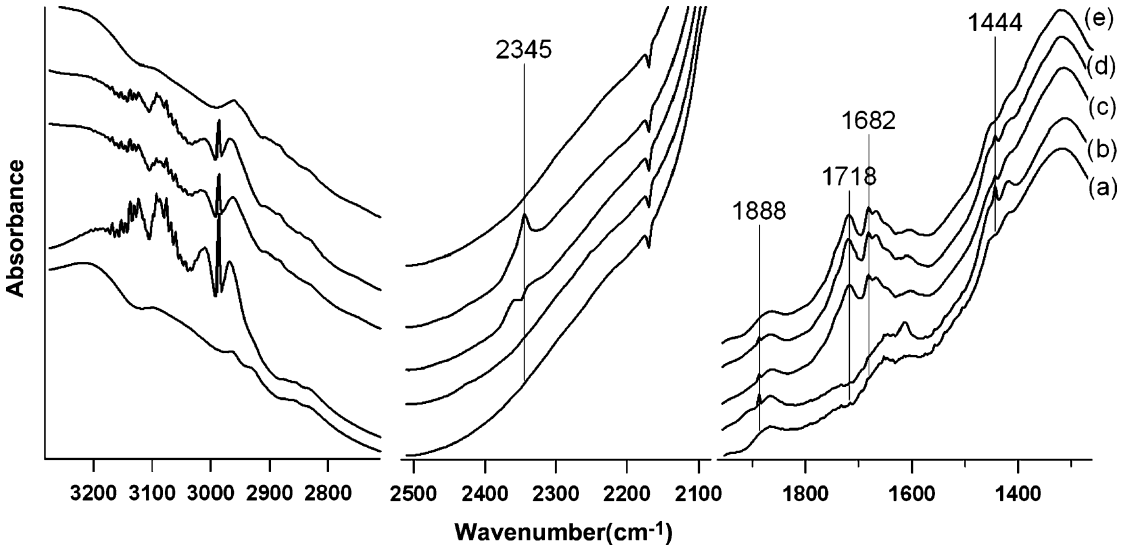

Fig. 9. IR spectra of ν(CH), ν(CO_2), ν(CO) regions for 0.1 M NH_4NO_3 treated AM-6 (a) under vacuum, (b) with 300 Torr C_2H_4 and O_2 in a 1 to 3 ratio, (c) after 10 h under UV, (d) after 30 min with UV lamp off, and (e) after evacuating reaction chamber.

peaks in the ν(C═O) region (1608, 1587 cm^{-1}) agree well with formic acid or carbonate species on the surface [36,37]. Formic acid or carbonate species were not observed on as-synthesized ETS-10 by Krisnandi et al. [35]. This difference could to be a result of the higher O_2 to C_2H_4 ratio used here. Our ETS-10 results also showed the formation of these peaks. Two new bands in the ν(C–H) region (2829, 2708 cm^{-1}) are present that have not been seen with ETS-10. These could correspond to methoxy species [37] or C–H stretches from acetic acid or acetaldehyde. All of these new bands remain after evacuation indicating that all these species are strongly absorbed in the micropores. The new absorption peaks on AM-6 show that the reaction of C_2H_4 with O_2 creates a number of partial oxidation products and it is not possible to definitively associate each band to a single product. However, the band for CO_2 formation around 2350 cm^{-1} is very distinct so that the catalyst's potential as a photocatalyst for VOC removal can be tested. In Fig. 7, however, the region around 2350 cm^{-1} is not shown since the as-synthesized AM-6 sample showed no peak for CO_2.

Ammonium exchanged ETS-10 (Fig. 8), gives rise to several strong peaks in the ν(C–H) region (2968, 2941, 2910, and 2883 cm^{-1}) after exposure to ethylene and O_2. These peak positions agree well with ethoxy groups on the surface, or possibly acetate ions at different sites in the structure [36,38]. The ν(C═O) region has two new peaks at 1552 and 1682 cm^{-1} along with the 1718 cm^{-1} peak (previously seen on AM-6 in Fig. 7), which all correspond to CO stretches in acetic acid or acetaldehyde at different sites in the structure. The 1682 cm^{-1} peak has been observed by Krisnandi et al. [23] and has been described by Escribano et al. [38] as a C═O stretch from acetaldehyde coordinated to a Lewis acid site through the oxygen, while the 1552 cm^{-1} peak may originate from the COO stretching in acetic acid, formic acid, or a carbonate species. The key difference between the NH_4^+ ion-exchanged ETS-10 and the as-synthesized ETS-10 for this reaction is the formation of CO_2 seen in Fig. 7 at 2345 cm^{-1}. This agrees with results from Krisnandi et al. [23,35] that show that more defective ETS-10 samples allow for complete oxidation of ethylene to CO_2 while the as-synthesized ETS-10 allows only partial oxidation (Fig. 9).

The reaction of ethylene with oxygen on ammonium-exchanged AM-6 shows the appearance of only three bands after 10 h under UV, the two associated with acetaldehyde at 1718 and 1682 cm^{-1}, and the CO_2 band at 2345 cm^{-1} (Fig. 9). No peaks were observed in the C-H region suggesting that any CH stretching in acetic acid or acetaldehyde is shifted by hydrogen bonding or is masked by the broad absorbance caused by the NH_4^+ ion exchange. The lack of peaks associated with partial oxidation products for treated AM-6 suggests that intermediates are not stable on NH_4^+ ion exchanged AM-6 and that the oxidation proceeds completely to CO_2. However, since there is a large change in coordination of the vanadium atoms down upon heating above 200 °C, it may be that the complete oxidation reflects the change in coordination in addition to the chemistry specific to vanadium. This interpretation is consistent with the results on NH_4^+ exchanged ETS-10, where it was seen that a more defective or damaged structure leads to complete oxidation.

4. Conclusions and summary

We have used a post-synthesis NH_4^+ ion exchange to modify ETS-10 and AM-6 and have compared the photocatalytic properties of these samples for ethylene oxidation. Our results are consistent with the reports of Krisnandi et al. [22,23] that NH_4^+ ion exchange introduces defects into the ETS-10 structure and that these defects allow for complete photooxidation of ethylene in oxygen to CO_2.

We have shown that the AM-6 UV/vis spectrum and the band gap energy do not red shift with ammonia ion exchange as they do for ETS-10; however changes were observed in the dehydrated exchanged AM-6 spectrum that indicate either a coordination or oxidation state change. There are similarities between the changes of Raman spectra for the V–O–V stretch in AM-6 and that of the Ti–O–Ti stretch in ETS-10. Both the Ti–O–Ti and V–O–V stretch largely disappear after NH_4^+ ion exchange. However, AM-6 retains a small IR signature of the V–O–V stretch and no new peak formed at higher frequency, indicating that the effects of ion exchange are different from those in ETS-10. We also observed further evidence for a coordination/oxidation state change in the dehydrated exchanged Raman spectrum of AM-6 with the formation of a new peak at 939 cm^{-1} that is assigned to a V═O bond.

We showed that heating the ion-exchanged AM-6 sample changes the coordination of the vanadium in the chain from an octahedral coordination to a tetrahedral coordination. Upon ammonia desorption, the H-AM-6 sample showed two new peaks associated with VOH groups in tetrahedrally coordinated vanadium. This dramatic change in coordination of the vanadium along

the chain however, did not cause the collapse of the AM-6 structure.

The reaction of ethylene in oxygen on the as-synthesized AM-6 sample showed partial oxidation of the ethylene to several possible products such as acetaldehyde, acetic acid, or formic acid. This result is similar to the results obtained from as-synthesized ETS-10 both here and by Krisnandi et al. [35], in that neither were able to completely oxidize ethylene to CO_2. After NH_4^+ ion exchange and dehydration, however both ETS-10 and AM-6 were shown to be able to completely oxidize ethylene to CO_2.

Acknowledgements

We thank J. Rabolt for use of Raman equipment and Anne-Marie Shough for her thoughtful discussions and insights on the AM-6 samples. Funding for this research was provided by the US Department of Energy Basic Energy Science program under grant no. DE-FG02-99ER14998.

References

[1] O.K. Dalrymple, D.H. Yeh, M.A. Trotz, J. Chem. Technol. Biotechnol. 82 (2007) 121.
[2] S. Malato, J. Blanco, D.C. Alarcon, M.I. Maldonado, P. Fernandez-Ibanez, W. Gernjak, Catal. Today 122 (2007) 137.
[3] J. Blanco-Galvez, P. Fernandez-Ibanez, S. Malato-Rodriguez, J. Sol. Energy: Trans. ASME 129 (2007) 4.
[4] K. Hashimoto, H. Irie, A. Fujishima, Jpn. J. Appl. Phys. 1 44 (2005) 8269.
[5] A.L. Linsebigler, G.Q. Lu, J.T. Yates, Chem. Rev. 95 (1995) 735.
[6] S. Anandan, A. Vinu, K.L.P.S. Lovely, N. Gokulakrishnan, P. Srinivasu, T. Mori, V. Murugesan, V. Sivamurugan, K. Ariga, J. Mol. Catal. A: Chem. 266 (2007) 149.
[7] S.T. Martin, C.L. Morrison, M.R. Hoffmann, J. Phys. Chem.-Us 98 (1994) 13695.
[8] M. Ni, M.K.H. Leung, D.Y.C. Leung, K. Sumathy, Renew. Sust. Energy Rev. 11 (2007) 401.
[9] S.M. Kuznicki, Large-pored Crystalline Titanium Molecular Sieve Zeolites, Engelhard Corporation, United States, 1989.
[10] M.W. Anderson, O. Terasaki, T. Ohsuna, A. Philippou, S.P. Mackay, A. Ferreira, J. Rocha, S. Lidin, Nature 367 (1994) 347.
[11] E. Borello, C. Lamberti, S. Bordiga, A. Zecchina, C.O. Arean, Appl. Phys. Lett. 71 (1997) 2319.
[12] K. Lazar, T.K. Das, K. Chaudhari, A.J. Chandwadkar, J. Catal. 125 (1999) 301.
[13] P. Brandao, A. Philippou, A. Valente, J. Rocha, M. Anderson, Phys. Chem. Chem. Phys. 3 (2001) 1773.
[14] P. Brandao, A.A. Valente, J. Rocha, M.W. Anderson, Stud. Surf. Sci. Catal. 142 (2002) 327.
[15] J. Rocha, P. Brandao, Z. Lin, M.W. Anderson, V. Alfredsson, O. Terasaki, Angew. Chem. Int. Ed. 36 (1997) 100.
[16] S. Uma, S. Rodrigues, I.N. Martyanov, K.J. Klabunde, Micropor. Mesopor. Mater. 67 (2004) 181.
[17] M.J. Nash, S. Rykov, R.F. Lobo, D.J. Doren, I. Wachs, J. Phys. Chem. C 111 (2007) 7029.
[18] A.M. Shough, R.F. Lobo, D.J. Doren, Phys. Chem. Chem. Phys. 9 (2007) 5096.
[19] A.M. Zimmerman, D.J. Doren, R.F. Lobo, J. Phys. Chem. B 110 (2006) 8959.
[20] A.M. Shough, D.J. Doren, M. Nash, R.F. Loho, J. Phys. Chem. C 111 (2007) 1776.
[21] F.X.L.I. Xamena, P. Calza, C. Lamberti, C. Prestipino, A. Damin, S. Bordiga, E. Pelizzetti, A. Zecchina, J. Am. Chem. Soc. 125 (2003) 2264.
[22] Y.K. Krisnandi, E.E. Lachowski, R.F. Howe, Chem. Mater. 18 (2006) 928.
[23] Y.K. Krisnandi, R.F. Howe, Appl. Catal. A: Gen. 307 (2006) 62.
[24] X.T. Gao, I.E. Wachs, J. Phys. Chem. B 104 (2000) 1261.
[25] S. Bordiga, G.T. Palomino, A. Zecchina, G. Ranghino, E. Giamello, C. Lamberti, J. Chem. Phys. 112 (2000) 3859.
[26] P.D. Southon, R.F. Howe, Chem. Mater. 14 (2002) 4209.
[27] B. Yilmaz, J. Warzywoda, A. Sacco, Nanotechnology 17 (2006) 4092.
[28] L.L.F. Su, X.S. Zhao, J. Porous Mater. 13 (2006) 263.
[29] L. Lv, F.B. Su, X.S. Zhao, Micropor. Mesopor. Mater. 76 (2004) 113.
[30] A. Zecchina, F.X.L.I. Xamena, C. Paze, G.T. Palomino, S. Bordiga, C.O. Arean, Phys. Chem. Chem. Phys. 3 (2001) 1228.
[31] S. Dzwigaj, P. Massiani, A. Davidson, M. Che, J. Mol. Catal. A: Chem. 155 (2000) 169.
[32] G. Centi, S. Perathoner, F. Trifiro, A. Aboukais, C.F. Aissi, M. Guelton, J. Phys. Chem.-Us 96 (1992) 2617.
[33] A. Jentys, N.H. Pham, H. Vinek, J. Chem. Soc. Faraday Trans. 92 (1996) 3287.
[34] A. Zecchina, S. Bordiga, G. Spoto, L. Marchese, G. Petrini, G. Leofanti, M. Padovan, J. Phys. Chem.-Us 96 (1992) 4991.
[35] Y.K. Krisnandi, P.D. Southon, A.A. Adesina, R.F. Howe, Int. J. Photoenergy 5 (2003) 131.
[36] J.R.S. Brownson, M.I. Tejedor-Tejedor, M.A. Anderson, J. Phys. Chem. B 110 (2006) 12494.
[37] J.R.S. Brownson, M.I. Tejedor-Tejedor, M.A. Anderson, Chem. Mater. 17 (2005) 6304.
[38] V.S. Escribano, G. Busca, V. Lorenzelli, J. Phys. Chem.-Us 94 (1990) 8945.